2000

Modeling Lithium Intercalation of a Single Spinel Particle under Potentiodynamic Control

Dong Zhang
University of South Carolina - Columbia

Branko N. Popov
University of South Carolina - Columbia, popov@engr.sc.edu

Ralph E. White
University of South Carolina - Columbia, white@cec.sc.edu

Publication Info

Journal of the Electrochemical Society, 2000, pages 831-838.

Publisher's link: http://dx.doi.org/10.1149/1.1393279
DOI: 10.1149/1.1393279

Journal of The Electrochemical Society, **147** (3) 831-838 (2000)
S0013-4651(99)06-099-1 CCC: $7.00 © The Electrochemical Society, Inc.

Modeling Lithium Intercalation of a Single Spinel Particle under Potentiodynamic Control

Dong Zhang,* Branko N. Popov, and Ralph E. White***,z**

Center for Electrochemical Engineering, Department of Chemical Engineering, University of South Carolina, Columbia, South Carolina 29208, USA

A mathematical model is presented for the lithium intercalation of a single spinel particle as a microelectrode under the stimulus of a cyclic linear potential sweep. The model includes both lithium diffusion within the particle and kinetics at the particle/electrolyte interface. The model is used to predict that peak current densities depend linearly on the scan rate to a certain power with a constant term, which is different from the predicted peak current density for a conventional redox system.

Manuscript submitted June 21, 1999; revised manuscript received October 19, 1999.

Although much has been done concerning the modeling of an electrode or a whole lithium battery, little can be found in the literature on the modeling of lithium intercalation of a single particle. West *et al.*[1] treated insertion into a composite cathode consisting of an active insertion material and electrolyte in a porous structure, modeling the electrolyte and active cathode material as superimposed continua without regard to microscopic structure. Mao and White[2] reformulated and extended their model to include a separator. The galvanostatic charge and discharge of a lithium anode/solid polymer separator/insertion cathode cell were modeled by Doyle *et al.*[3] Later Fuller *et al.*[4] presented a mathematical model for the galvanostatic charge and discharge of a dual lithium insertion (rocking-chair) cell. Paxton and Newman[5] proposed a theoretical approach for estimating a constant diffusion coefficient to use in an insertion electrode model for the case where experimental data exist for the diffusion coefficient as a function of state of charge of an intercalation material.

Carefully controlled experiments and theoretical analyses are needed to clarify the behavior of individual components (*i.e.*, active material, conductive filler, and binder) that make up a typical porous electrode that is used in a cell. Individual carbon-fiber electrodes were used by Verbrugge and Koch[6,7] to isolate characteristics intrinsic to a lithiated carbon fiber. They also proposed a theoretical approach and mathematical methods in cylindrical geometry to investigate lithium intercalation of single-fiber carbon electrodes.

Microelectrode techniques make it possible to determine the kinetic and transport properties of lithium insertion/extraction of a particle with a diameter of 10 to 100 μm. [8-10] Microelectrode techniques are very versatile in kinetic studies because of high rates of flux in the electrolyte phase due to the small size of the electrode, less interference by resistive polarization, and less capacitive current due to the double layer capacity.[11,12] Furthermore, the results are not complicated by the influence of binders, electronically conductive additives, or other components necessary for the fabrication of porous electrodes. In other words, the response is solely from the reaction between the active material and the electrolyte. The current observed in the voltammetry for a microelectrode is typically on the order of nanoamperes, which is four to six orders of magnitude smaller than the usual current observed in cyclic voltammetry experiments. This is due to the small surface area of the particle electrode. This feature reduces greatly the distortion of cyclic voltammetric behavior due to ohmic resistance, which is found in studies of porous electrodes.

This paper describes an approach to simulate mathematically the behavior of lithium intercalation in a spinel particle including both mass transport within the particle and kinetics at the particle/electrolyte interface subject to a potentiodynamic stimulus.

* Electrochemical Society Student Member.
** Electrochemical Society Active Member.
*** Electrochemical Society Fellow.
z E-mail: white@engr.sc.edu

Model Development

The following assumptions apply when we simulate the lithium extraction/insertion behavior of a spherical particle following application of a potentiodynamic stimulus. (*i*) Radial diffusion of lithium ions dominates the process. In other words, the lithium concentration gradient in the particle occurs only in the radial direction. (*ii*) A Butler-Volmer reaction rate expression governs the charge-transfer kinetics at the electrode/electrolyte interface. (*iii*) The open-circuit potential of lithium intercalation includes two plateaus, as given by Eq. A-1 in the Appendix and shown in Fig. A-1. (*iv*) Current for the charge and discharge of double layer capacitance at the solid-electrode/liquid interface is neglected. (*v*) There are no side reactions such as electrolyte decomposition. The electrode/electrolyte interfacial kinetics are not complicated by solid electrolyte interphase (SEI) formed on the electrode surface. (*vi*) The Li^+ concentration in the electrolyte is constant. (*vii*) The electrochemical reaction that occurs at the surface of the particle can be represented as

$$Li^+ + e^- + Mn_2O_4 \underset{\text{deintercalation, charge}}{\overset{\text{intercalation, discharge}}{\rightleftharpoons}} LiMn_2O_4 \quad [1]$$

According to Reaction 1, lithium ions are intercalated into solid manganese dioxide in which manganese is in the +4 oxidation state and reduce the oxidation state of Mn to 3.5, as shown on the right side of Reaction 1. (*viii*) The flux of the lithium ions within the sphere is due to diffusion in a concentration gradient field. (*ix*) There is no phase change of the crystalline particle during intercalation or deintercalation of lithium ions. (*x*) The lithium ion diffusion coefficient D is a constant. (*xi*) There are no pores inside the particle. That is, it is a perfect solid sphere.

In general, the intercalation of lithium ions into a spinel particle can be described in terms of a process in which a lithium ion in the solution adjacent to the electrode becomes partially desolvated and adsorbed onto the surface of the microelectrode; this process is accompanied by the insertion of an electron into the conduction band of the solid. Subsequently, the partially solvated Li^+ ion moves across or along the surface to an intercalation site, where it becomes fully desolvated and enters the lattice as an ion (and at the same time, the oxidation state of transition metal ions is lowered).[13-15] Thereon the lithium ions occupying the sites close to the surface of the particle diffuse radially into the center of the particle by the driving force of a concentration gradient. The deintercalation of lithium ions is considered to be a process opposite to the above description.

The flux of lithium ions ($\mathbf{N}$) within the particle is

$$\mathbf{N} = -D\nabla c \quad [2]$$

where c is the concentration of lithium ions and D is diffusion coefficient. Diffusion is assumed to be the mechanism of transport of the lithium ion in the particle.

S0013-4651(99)06-099-1 CCC: $7.00 © The Electrochemical Society, Inc.

A material balance for a small volume element in the particle leads to the differential conservation law for Li^+ in the particle

$$\frac{\partial c}{\partial t} = -\nabla \cdot \mathbf{N} \quad [3]$$

The combination of Eq. 2 and 3 yields

$$\frac{\partial c}{\partial t} = D\,\nabla^2 c \quad [4]$$

We start from the fully discharged state as an initial condition with uniform lithium concentration c_0 in the particle, corresponding to the composition $Li_{1.0}Mn_2O_4$, and finite kinetics are considered. We wish to keep the model general thus the interfacial kinetics of the electrode is included. For a single spherical electrode, the governing equations are

1. Fick's second law

$$\frac{\partial c}{\partial t} = D\left(\frac{\partial^2 c}{\partial r^2} + \frac{2}{r}\frac{\partial c}{\partial r}\right) \quad [5]$$

where r is radial distance from the center of the particle.

2. Initial condition

$$c(r, 0) = c_0 \quad [6]$$

3. At the electrode surface

$$\frac{i}{F} = -D\left(\left.\frac{\partial c}{\partial r}\right|_{r=r_0}\right) \quad [7]$$

where i is the current density at the electrode surface and is positive during deintercalation of lithium ions.

The current density i is assumed to be given by a Butler-Volmer equation with Eq. 1 as the reaction mechanism[4,16]

$$\frac{i}{F} = k(c_1)^{1-\beta}(c_\theta)^{1-\beta}(c_s)^{\beta}\left\{\exp\left(\frac{1-\beta F\eta}{RT}\right) - \exp\left(-\frac{\beta F\eta}{RT}\right)\right\} \quad [8]$$

Combination of Eq. 7 and 8 yields

$$-D\left(\left.\frac{\partial c}{\partial r}\right|_{r=r_0}\right) = k(c_1)^{1-\beta}(c_\theta)^{1-\beta}(c_s)^{\beta}\left\{\exp\left(\frac{(1-\beta)F\eta}{RT}\right) - \exp\left(-\frac{\beta F\eta}{RT}\right)\right\} \quad [9]$$

or

$$-FD\left(\left.\frac{\partial c}{\partial r}\right|_{r=r_0}\right) = i_0\left\{\exp\left(\frac{(1-\beta)F\eta}{RT}\right) - \exp\left(-\frac{\beta F\eta}{RT}\right)\right\} \quad [10]$$

and

$$i_0 = Fk(c_1)^{1-\beta}(c_\theta)^{1-\beta}(c_s)^{\beta} \quad [11]$$

where r_0 is the radius of the particle, k is a reaction rate constant, c_l is the Li^+ concentration in the liquid phase (treated here as a constant, known value), c_θ ($= c_t - c_s$) is the surface concentration of vacant sites ready for lithium intercalation, c_s is the concentration of lithium ions on the surface of the electrode, and c_t is the concentration of total sites for seating lithium ions. The overpotential η is defined as

$$\eta = \varphi_s - U \quad [12]$$

where φ_s is the potential at the surface of the particle and U is the open-circuit potential of the electrode, which is a function of the concentration of lithium ions in the particle.

4. At the center of the spherical electrode

$$\left.\left(\frac{\partial c}{\partial r}\right)\right|_{r=0} = 0 \quad [13]$$

To make the problem simpler, we suppose that the potential φ is uniform throughout the particle. Thus

$$\varphi_s = U_{app} \quad [14]$$

where U_{app} is the applied potential. This is a reasonable assumption because the specific conductivity of the spinel[17] is $10^{-4}\ \Omega^{-1}\ cm^{-1}$. Thus, for a particle with radius of 10 μm, the voltage difference between the center and the surface of the particle can be estimated by using Ohm's law to be less than 5 mV with a current density of 0.6 mA/cm^2, which will cause only a small deviation for the voltammetric responses under investigation.

The governing equation, initial condition, and boundary conditions can be placed in a convenient dimensionless form if we use the following dimensionless variables

$$\text{dimensionless time } \tau = \frac{tD}{r_0^2} \quad [15]$$

$$\text{dimensionless distance from the center of particle } x = \frac{r}{r_0} \quad [16]$$

$$\text{dimensionless concentration } y = \frac{c}{c_0} \quad [17]$$

$$\text{and dimensionless current density } j = \frac{ir_0}{FDc_0} \quad [18]$$

Equations 5, 6, 7, and 13 become

$$\frac{\partial y}{\partial \tau} = \frac{\partial^2 y}{\partial x^2} + \frac{2}{x}\frac{\partial y}{\partial x} \quad [19]$$

$$y(x, 0) = 1 \quad [20]$$

$$j = -\left(\left.\frac{\partial y}{\partial x}\right)\right|_{x=1} \quad [21]$$

$$\left.\left(\frac{\partial y}{\partial x}\right)\right|_{x=0} = 0 \quad [22]$$

If we let $c_0 = c_t$, that is, the initial concentration is equal to the total concentration, Eq. 10 becomes

$$\left.\left(\frac{\partial y}{\partial x}\right)\right|_{x=1} + a\left(y|_{x=1}\right)^{\beta}\left(1 - y|_{x=1}\right)^{1-\beta}\left\{\exp\left(\frac{(1-\beta)F\left(U_{app} - U\right)}{RT}\right) - \exp\left(-\frac{\beta F\left(U_{app} - U\right)}{RT}\right)\right\} = 0 \quad [23]$$

where $y|_{x=1} = c_s/c_t$ and

$$a = \frac{kr_0c_l^{1-\beta}}{D} \quad [24]$$

which is a dimensionless parameter denoting the ratio of the diffusional resistance (r_0/D) to the interfacial kinetic resistance $\{1/(kc_l^{1-\beta})\}$, involving the Li^+ concentration in the liquid phase. Under potentiodynamic stimulus, the applied potential changes linearly with time, and can be expressed by

$$U_{app} = U_0 + vt \quad [25]$$

S0013-4651(99)06-099-1 CCC: $7.00 © The Electrochemical Society, Inc.

Table I. Parameters for the lithium intercalation reaction.

D (cm^2 s^{-1})	2.2×10^{-9}
β	0.5
c_l (mol dm^{-3})	1.0
r_0 (cm)	5×10^{-4}
c_0 (mol dm^{-3})	23.7
c_t (mol dm^{-3})	23.7
c_θ (mol dm^{-3})	0.0 (initial value)
k (cm$^{5/2}$ s^{-1} mol$^{-1/2}$)	0.00019
v (mV s^{-1})	1.0
a (dimensionless)	1.36
U_0 (V) ($y\|_{x=1} = 1.0$)	3.5102

Table II. Parameters for the lithium intercalation reaction.

D (cm^2 s^{-1})	10^{-9}
β	0.5
c_l (mol dm^{-3})	1.0
r_0 (cm)	5×10^{-4}
c_0 (mol dm^{-3})	23.7
c_t (mol dm^{-3})	23.7
c_θ (mol dm^{-3})	0.0 (initial value)
k (cm$^{5/2}$ s^{-1} mol$^{-1/2}$)	0.0001
a (dimensionless)	1.58
U_0 (V) ($y\|_{x=1} = 1.0$)	3.5102

where U_{app} is the applied potential, U_0 is the initial applied potential, which we assign to be the same as the initial open-circuit potential and is further discussed below. The potential sweep rate is represented as v.

Equations 19, 20, 22, and 23 with assigned parameters in Table I or II were solved with a partial differential equation solver PDE2D.[18] Among the features of this solver are employment of a collocation method with cubic Hermite basis functions, adaptive time step control and discretization of time by use of the Crank-Nicolson scheme. The dimensionless current density of lithium insertion/extraction is given by Eq. 21. Since the open-circuit potential for reaction 1 is non-Nernstian, Eq. 23 is complicated. The open-circuit potential expression (see the Appendix) for Reaction 1 was given by Doyle *et al*.[16] In this simulation the applied potential range, U_{app}, is from 3.5102 to 4.3102 V *vs*. Li/Li$^+$.

Results and Discussion

Comparison of simulation results with experimental data.—Figure 1 presents a comparison of our model predictions to experimental data.[10] The predicted dimensionless current density j is obtained by solving the governing equations with the parameter values given in Table I. The predictions for j were made by beginning the potential sweep at $t = 0$ with $U_{app} = 3.5102$ V so that $j = 0$ since $U_{app} = U|_{y=1} = 3.5102$ V. Then by incrementing time U_{app} is increased by 1 mV per second and j is obtained by solving the equations. Note that U_{app} in this case is slightly larger than U so that the anodic portion of the Butler-Volmer equation (first term in the curly brackets in Eq. 23) is positive. As can be seen in Fig. 1, an anodic peak in the predicted dimensionless current density occurs at about 3.98 V, which is just above the lower voltage plateau in Fig. A-1. As time proceeds, the applied potential is incremented until a second dimensionless current density peak is predicted to occur at a voltage of about 4.12 V, which is just above the upper voltage plateau in Fig. A-1. The predicted dimensionless current density then drops after this second peak because the applied potential is very nearly equal to the open-circuit potential (see Fig. A-1). Note that the predicted dimensionless concentration of lithium ions at the surface of the particle ($y|_{x=1}$) is also obtained by solving the equations at each time step. Once the applied potential is raised to 4.3102 V, the direction of the sweep is changed by changing the sign of v to a minus sign. Now, as time proceeds, U_{app} is reduced from 4.1302 V, and this provides a predicted cathodic peak in the dimensionless current density j at about 4.11 V. The predicted current density is negative now because the applied potential is slightly less than the open-circuit potential so that the cathodic portion of the Butler-Volmer equation (last term on the right in the brace in Eq. 23) is now greater than the

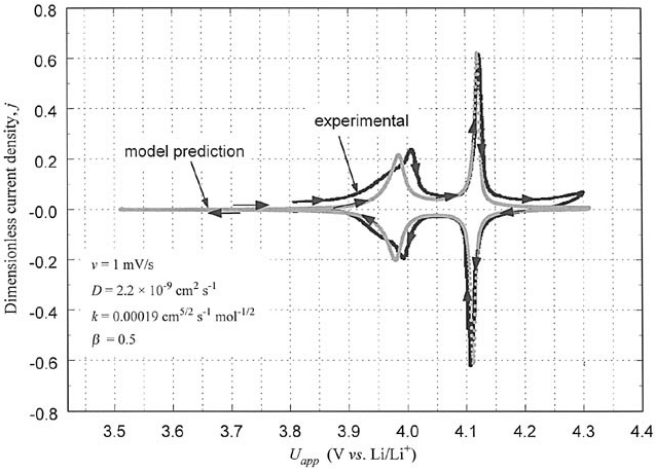

Figure 1. Comparison of model predictions with experimental data.[10] Parameter values are given in Table I.

Table III. Diffusion coefficients of lithium-ion in $Li_yMn_2O_4$.

D (cm^2 s^{-1})	y	Method[a]	Ref.
0.5 to 1.5 × 10^{-9}	0 and 0.5 ≤ y ≤ 1	PITT	19
10^{-11}	0.4	Transient	21
0.66 to 1.4 × 10^{-10}	0.1 ≤ y ≤ 0.8	PSCA in an aqueous phase	22
0.19 to 3.1 × 10^{-11}	0.1 ≤ y ≤ 0.8	EIS in an aqueous phase	23
4.89 × 10^{-9}	0.2 ≤ y ≤ 0.8	CV	20
9.65 × 10^{-10}	0.3	EIS	24
0.092 to 2.0 × 10^{-12}	0.1 ≤ y ≤ 0.5	EIS	25
2.2 × 10^{-9}	0.17 ≤ y ≤ 1.0	CV	This paper

[a] Nonaqueous electrolyte except as indicated.
PITT: potentiostatic intermittent titration technique.
PSCA: potential step chronoamperometry.
EIS: electrochemical impedance spectroscopy.
CV: cyclic voltammetry.

S0013-4651(99)06-099-1 CCC: $7.00 © The Electrochemical Society, Inc.

anodic portion. As time continues, a second cathodic peak is predicted to occur at about 3.98 V, as expected.

The qualitative agreement between the predictions and the measured values of j in Fig. 1 was obtained by a trial-and-error adjustment of the parameters D and k (after fixing $\beta = 0.5$) so that the predicted peak potentials and peak current densities agreed reasonably well with the experimental data, as shown in Fig. 1. The value for D obtained here ($D = 2.2 \times 10^{-9}$ cm^2 s^{-1}) is similar to those obtained by Guyomard and Tarascon[19] ($D = 0.5$ to 1.5×10^{-9} cm^2 s^{-1}) and by Xia and Yoshio[20] ($D = 4.89 \times 10^{-9}$ cm^2 s^{-1}). The literature values of the diffusion coefficient of lithium-ion in spinel $Li_yMn_2O_4$ are summarized in Table III. It is seen in this table that the D values vary over four orders of magnitude, indicating that disagreement exists in the literature. The discrepancy between the two curves in Fig. 1 may be due to the extended cycling of the spinel electrode for the experimental data or the fact that the geometry of the experimental spinel particle is not perfectly spherical. Other causes could be that the lithium diffusion coefficient D varies with the state of charge of the particle or that the open-circuit potential of the spinel particle used in the experiment may be somewhat different from the expression we used (Appendix).

Features of the simulation results.—Figure 2 shows the simulation results with the parameters from Table II, which are slightly different from those in Table I. The upper case letters in Fig. 2 correspond to the concentration profiles in Fig. 3, which shows the predicted concentration profiles at different times using the parameters in Table II at a scan rate of 0.4 mV/s. The upper case letters in this figure correspond to the points in Fig. 2. The concentration distribution and the concentration gradient at the particle surface change drastically during the anodic and cathodic process. Initially the concentration is uniform at 1.00 (dimensionless) or 23.7 mol/dm^3 as shown in Fig. 3a. During the anodic (charging, deintercalating) process, with a linear increase of the applied potential, lithium deintercalation occurs, and lithium ions flow out of the particle, which increases the oxidation state of Mn from 3.5 to 4. Consequently, the average concentration of lithium ions within the particle keeps decreasing. The concentration gradient is seen very obviously when time reaches the positions of current density peaks (D and F in Fig. 2 and 3 when $\tau = 4.8$ or $\tau = 6.24$, corresponding to $U_{app} = 3.990$ and 4.134 V, respectively); at other times, the gradient is relatively small. The concentration profiles for the cathodic (discharging, intercalating) process during the back sweep of the applied potential are similar to those for the anodic process, except that the average concentration increases and the direction of the concentration gradient, corresponding to intercalating lithium into the particle, is opposite to the anodic process, as shown in Fig. 3b. Again, the concentration gradient at the particle surface reaches its maxima when the applied potential is at the cathodic peak current density positions at $\tau =$ 10.08 or $\tau = 11.52$, corresponding to $U_{app} = 4.102$ and 3.958 V, respectively (K and N in Fig. 2 and 3).

Cyclic voltammograms for various scan rates v.—Figure 4a shows the first cycle voltammograms for scan rates of 0.2 to 6.4 mV/s over the applied potential, U_{app}, range from 3.51 to 4.31 V

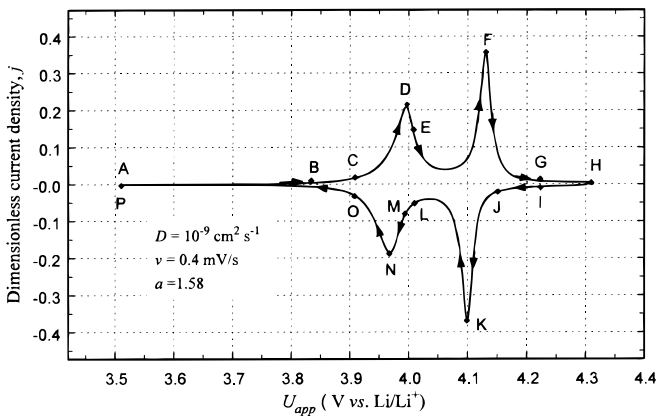

Figure 2. Comparison of calculated cyclic voltammograms of cycle 1 and cycle 10 with $v = 0.4$ mV/s. The points specified by upper case letters correspond to the concentration profiles in Fig. 3.

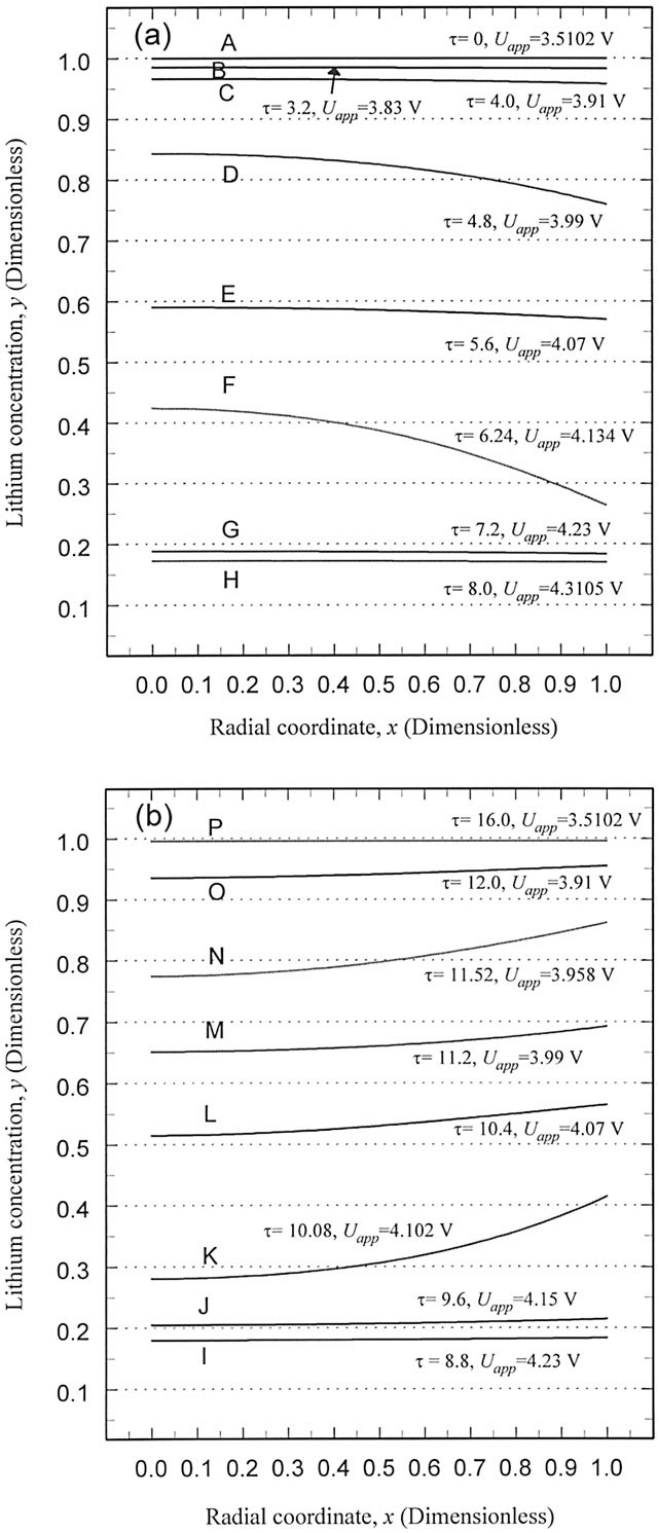

Figure 3. Concentration profiles of lithium within the spinel particle at scan rate 0.4 mV/s. (a) Anodic (charging, deintercalating) process, (b) cathodic (discharging, intercalating) process. The uppercase letters in this figure correspond to the points in Fig. 2.

S0013-4651(99)06-099-1 CCC: $7.00 © The Electrochemical Society, Inc.

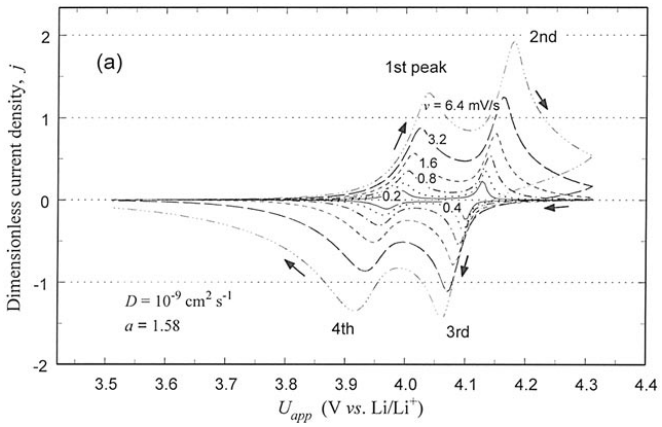

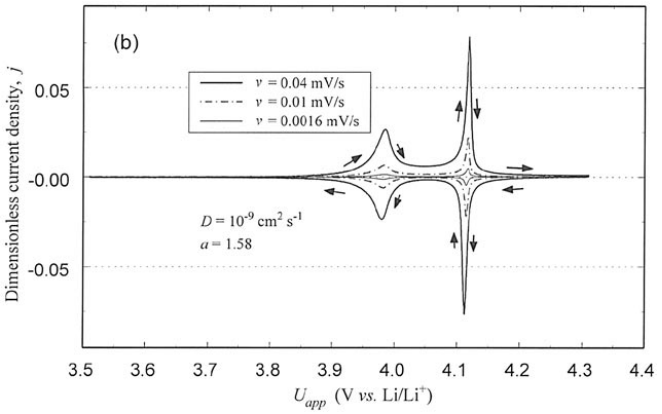

Figure 4. Cyclic voltammograms for various scan rates with $a = 1.58$ and $\beta = 0.5$. (a) $v = 0.2$ to 6.4 mV/s, (b) $v = 0$ to 0.04 mV/s.

vs. Li/Li^+ and back. As can be seen in Fig. 4a, the peaks in the anodic dimensionless current densities become larger and the potentials associated with those peaks become more positive, and the cathodic peak dimensionless current densities become more negative and those associated potentials becomes more negative for larger sweep rates. To see clearly the change of cyclic voltammograms when varying the potential scan rate, the values of the dimensionless peak current density and associated potential from Fig. 4a are summarized in Table IV. The first anodic peak current density is 0.116 at the potential scan rate of 0.2 mV/s, compared to the anodic dimensionless peak current density of 1.296 at the potential scan rate of 6.4 mV/s. In a similar manner, the first anodic peak potential *vs.* Li/Li^+ changes from 3.992 V at a scan rate of 0.2 mV/s to 4.040 V at a scan rate of 6.4 mV/s. The shape and position of the other anodic and cathodic peaks vary with v similarly. As a result of the shift of the dimensionless current density peaks, the difference between the values of the peak potential of corresponding peaks becomes larger, indicating the existence of charge-transfer resistance and non-Nernstian behavior of the system under study. Since the peak height and shape of the cyclic voltammograms for $v \leq 0.2$ mV/s are much different from those at scan rates above 0.2 mV/s, Fig. 4b presents the predicted voltammograms for scan rates 1.6×10^{-3} to 4×10^{-2} mV/s.

To correlate the dimensionless peak current density with scan rate, the first anodic peak current density j_{p1} values given in Table IV are plotted as a function of $v^{1/2}$ in Fig. 5a. The formation of this peak current density has exactly the same initial conditions for the various scan rates. Apparently the relationship of j_{p1} *vs.* $v^{1/2}$ is linear when $v > 0.2$ up to 10 mV/s. Mean square regression of the values for $v^{1/2} \geq 0.5$ mV/s gives

$$j_{p1} = 0.575v^{1/2} - 0.158 \quad [26]$$

This relationship is in agreement with some literature values in that an equation like Eq. 26 was used to estimate the diffusion coefficient of lithium ions in the spinel phase of a thin, porous electrode.[20,22] However, the present model predicts that extrapolation of the linear relationship to a very low scan rate (say, $v < 0.05$ mV/s) is not appropriate, since theoretically if the scan rate is infinitely small the peak current density should be close to zero. In other words, j_{p1} *vs.* $v^{1/2}$ is nonlinear over very low scan rates. The dashed line in Fig. 5a is a curve depicting the relation at very low scan rates, corresponding to the first anodic peaks in Fig. 4b (also, see Table IV). The equation $j_p = \lambda v^{1/2}$, where λ is a constant related to charge-transfer coefficient and lithium diffusion coefficient, with no constant term as used by Xia and Yoshio[20] and Ooi *et al.*[22] does not agree with the model predictions presented here. This is because (*i*) the thermodynamics of the lithium intercalation of spinel departs from the Nernst equation[26] which was the precondition for the derivation of the relationships used by Ooi *et al.* or Xia and Yoshio; (*ii*) at very low scan rates, the particle will show a lumped response, and the current will be proportional to the scan rate.

Figure 5b shows the second anodic peak dimensionless current density as a function of the scan rate to the power of 0.63. As shown in Fig. 5b, these second peaks do not depend in a linear manner on the square root of the scan rate as do the first peaks above a certain scan rate. The predicted dimensionless peak current density dependence on scan rate presented here agrees well with that reported by Uchida *et al.*[10] They determined experimentally that the second peak current density was proportional to $v^{0.7\text{-}0.8}$

To show the effect of the upper plateau of the open-circuit potential on the third dimensionless peak current density, we ran the model by starting the scans in the cathodic direction at 4.3102 V with an initial dimensionless concentration (y) of 0.17 instead of using a starting potential of 3.5102 V (with $y = 1.00$) and then scanning anodically, as done above. Thus, the initial conditions are the same for all scan rates for the cathodic scans shown in Fig. 6. Comparison of Fig. 6 to Fig. 4 reveals that for all the scan rates in Fig. 6

Table IV. Predicted peak dimensionless current densities and peak potentials for various scan rates.

v (mV/s)	j_p (dimensionless)				U_{app} *vs.* Li/Li^+ (V)			
	Anodic		Cathodic		Anodic		Cathodic	
0.0016	0.00141	0.00481	−0.00455	−0.00125	3.982	4.117	4.114	3.981
0.01	0.00673	0.0229	−0.0227	−0.00599	3.982	4.117	4.113	3.981
0.04	0.0251	0.0783	−0.0764	−0.0236	3.985	4.119	4.112	3.979
0.2	0.116	0.229	−0.231	−0.109	3.992	4.127	4.098	3.968
0.4	0.209	0.355	−0.361	−0.188	3.996	4.132	4.093	3.963
0.8	0.353	0.537	−0.551	−0.309	4.007	4.142	4.089	3.958
1.6	0.567	0.807	−0.789	−0.514	4.011	4.151	4.079	3.949
3.2	0.875	1.246	−1.116	−0.841	4.025	4.161	4.069	3.934
6.4	1.296	1.932	−1.448	−1.350	4.040	4.180	4.059	3.915

S0013-4651(99)06-099-1 CCC: $7.00 © The Electrochemical Society, Inc.

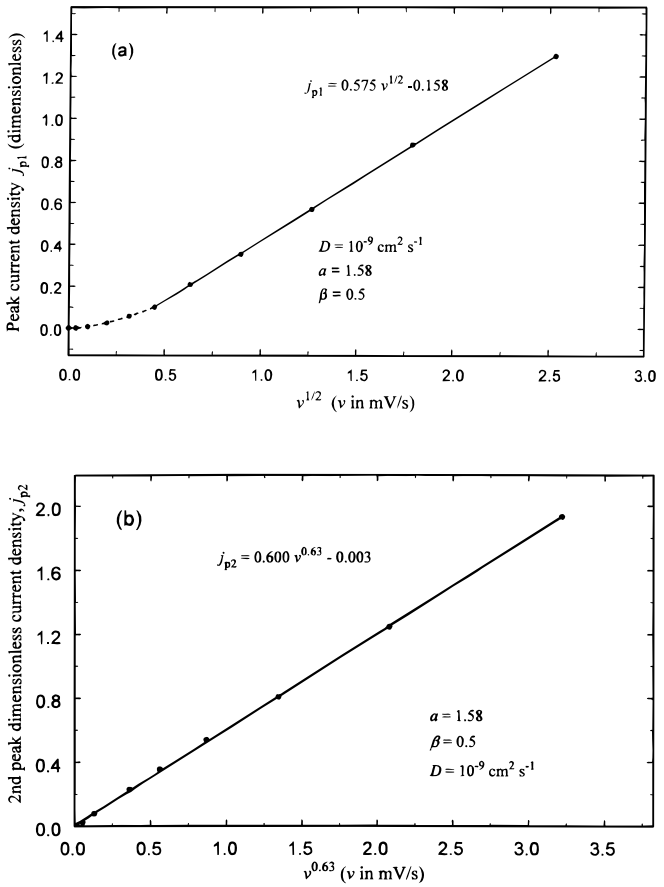

Figure 5. Peak dimensionless current density as a function of the scan rate to a certain power for (a) the first peak and (b) the second peak. The values used in (a) and (b) are derived from Fig. 4.

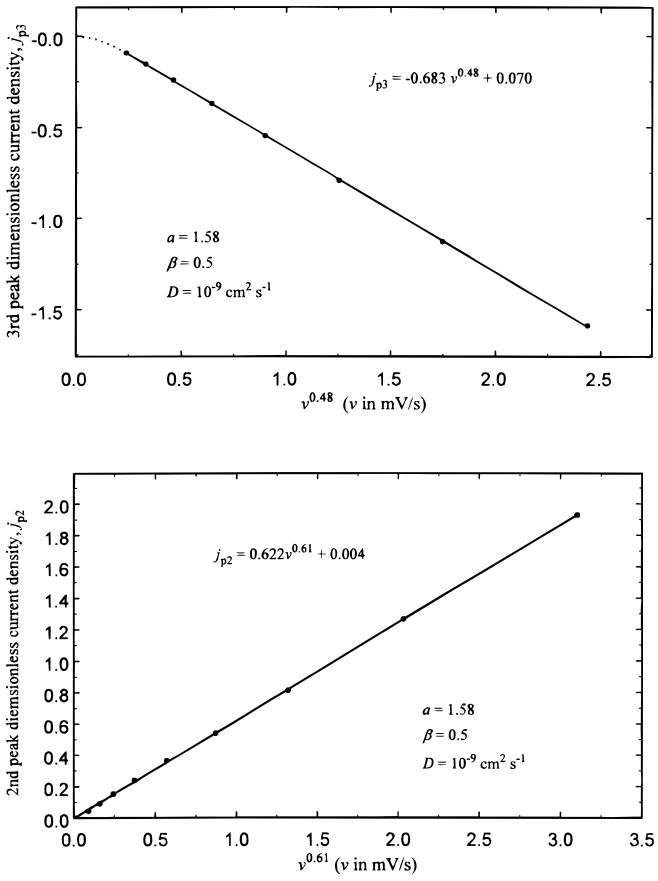

Figure 7. The peak dimensionless current density as a function of the scan rate to a certain power for (a) the third peak and (b) the second peak. The values are derived from the voltammograms predicted for the scans started at 4.3102 V as shown in Fig. 6.

the dimensionless current density is zero at 4.3102 V, which is different from the values shown in Fig. 4 at the same potential. Figure 7a shows that the cathodic peak dimensionless current density j_{p3} is proportional to $v^{0.48}$, when $6.4 \geq v \geq 0.05$ mV/s. This dependence of j_{p3} on $v^{0.48}$ indicates that the formation of a peak dimensionless current density on discharge (intercalation) is similar to a redox system in an aqueous solution.[26]

Figure 7b shows the second anodic peak current density as a function of $v^{0.61}$ for the voltammograms predicted for the scans started at 4.3102 V in the cathodic direction. Note that there is only a slight difference between Fig. 5b and Fig 7b. This slight difference is due to the two different starting points (3.5102 and 4.3102 V, respectively) for the scans.

To demonstrate the effect of the upper plateau of the open-circuit potential on the second peak dimensionless current density, we ran the model by starting the scans in the anodic direction at 4.0602 V with an initial dimensionless concentration (y) of 0.5806. This initial point is the midpoint between the lower plateau and the upper plateau. As a result, the formation of all of the second peaks has the same initial conditions. Figure 8 shows the voltammograms obtained this way. Comparison of Fig. 8 to Fig. 4 reveals that for all the scan rates in Fig. 8 the dimensionless current density is zero at 4.0602 V where the anodic scans were started. Figure 9 shows that the anodic peak dimensionless current density j_{p2} is proportional to $v^{0.45}$, when $6.4 \geq v \geq 0.05$ mV/s.

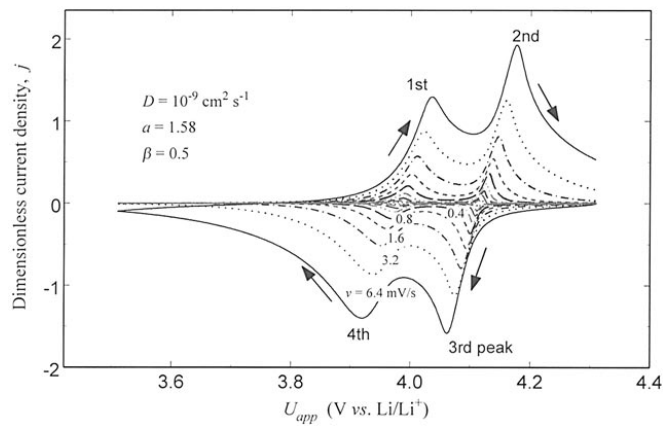

Figure 6. The voltammograms with the scans starting from 4.3102 V for various scan rates.

Cyclic voltammograms for different values of a.—In the boundary condition 23, a is a dimensionless parameter denoting ratio of diffusional resistance of lithium in the solid host to interfacial kinetic resistance, involving the Li^+ concentration in the liquid phase. Equation 24 gives the mathematical expression for this parameter. Larger a means faster interfacial charge-transfer kinetics when the diffusion coefficient is fixed. On the other hand, when the interfacial reaction constant k is kept at a certain value, smaller a means faster diffusion of lithium in the solid host. Figure 10 shows the cyclic voltammograms for various values of a at the scan rate of 0.4 mV/s. In Fig. 10 the parameter a was changed by changing parameter k. The shapes of the cyclic voltammograms change appreciably when parameter a is increased from 0.0316 to 3.16. For instance, the first anodic peak potential decreases from $U_{app} = 4.113$ V *vs.* Li/Li$^+$ for $a = 0.0316$ to 3.992 V *vs.* Li/Li$^+$ for $a = 3.16$; at the same time, the value of the dimensionless first anodic peak current density increas-

S0013-4651(99)06-099-1 CCC: $7.00 © The Electrochemical Society, Inc.

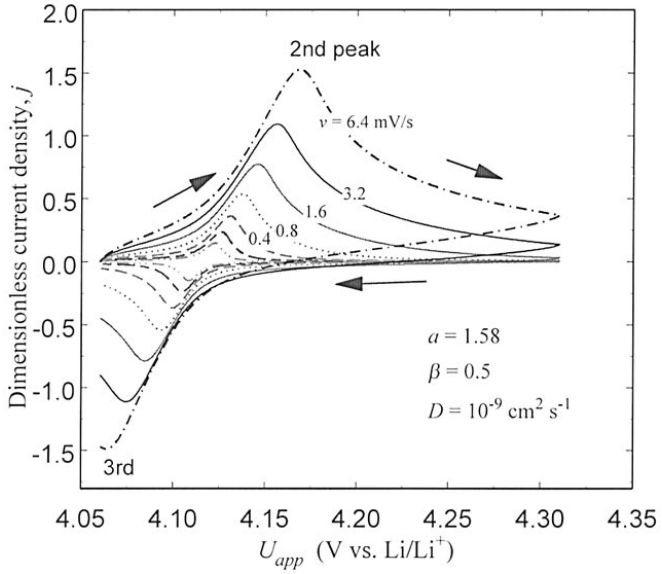

Figure 8. The voltammograms by starting the scans in the anodic direction at 4.0602 V with an initial dimensionless concentration (y) of 0.5806.

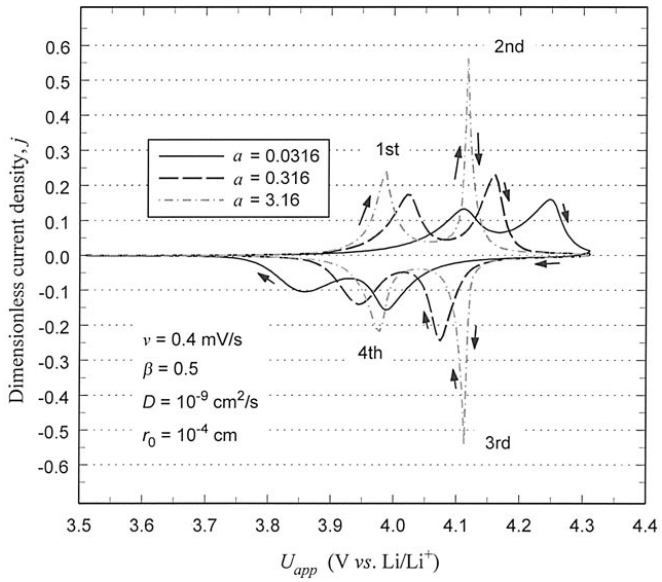

Figure 10. Cyclic voltammograms for various values of a at scan rate v = 0.4 mV/s and β = 0.5 by changing k.

es from 0.133 for a = 0.0316 to 0.217 for a = 3.16. However, a further increase of a results in only a little decrease in the first anodic peak potential, 3.987 V *vs*. Li/Li^+ for a = 31.6 and 3.986 V *vs*. Li/Li^+ for a = 3160. Simultaneously, the dimensionless first anodic peak current density increases to 0.223 for a = 31.6 and 0.224 for a = 3160. Similar behavior was observed for other current density peaks. The little change of peaks at high a values reflects that when the interfacial reaction kinetics is very fast, the whole intercalation process is controlled by the lithium diffusion in the solid host, as expected.

Cyclic voltammograms for different values of β.—β is a symmetry factor representing the fraction of the applied potential U_{app} which promotes the cathodic reaction. In most cases β is close to 0.5. Variation of β will lead to appreciable deformation of cyclic voltammograms, especially when the interfacial kinetics is important in the lithium intercalation process. Figure 11 shows our predicted voltammetric responses for various values of β when v = 0.4 mV/s. For this large value of a the deformation of cyclic voltammograms is not very distinct, as shown in Fig. 11a; however, there are significant changes in the curves for various values of β when a is small as shown in Fig. 11b. It can be seen in Fig. 11b that a decrease of β favors the anodic reaction and makes the values of peak potential smaller. Furthermore, a decrease of β results in an increase of the values of anodic peak dimensionless current density and a decrease of the values of cathodic peak dimensionless current densities. By fitting the present model to experimental data, it should be feasible to acquire a precise β value for a lithium intercalation of a specific spinel.

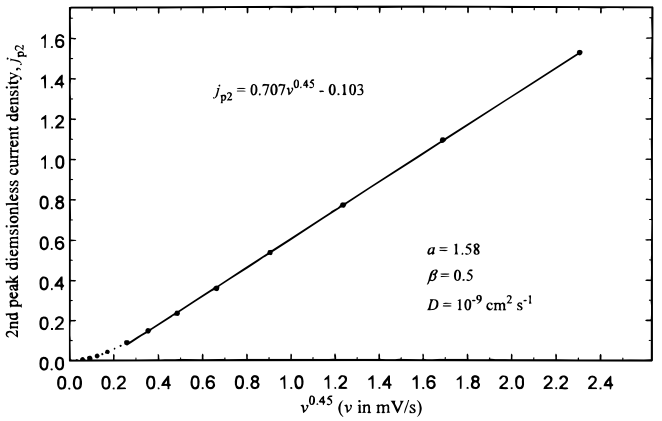

Figure 9. Second anodic peak dimensionless current density j_{p2} as a function of $v^{0.45}$. The values are derived from the voltammograms predicted for the scans started at 4.0602 V as shown in Fig. 8.

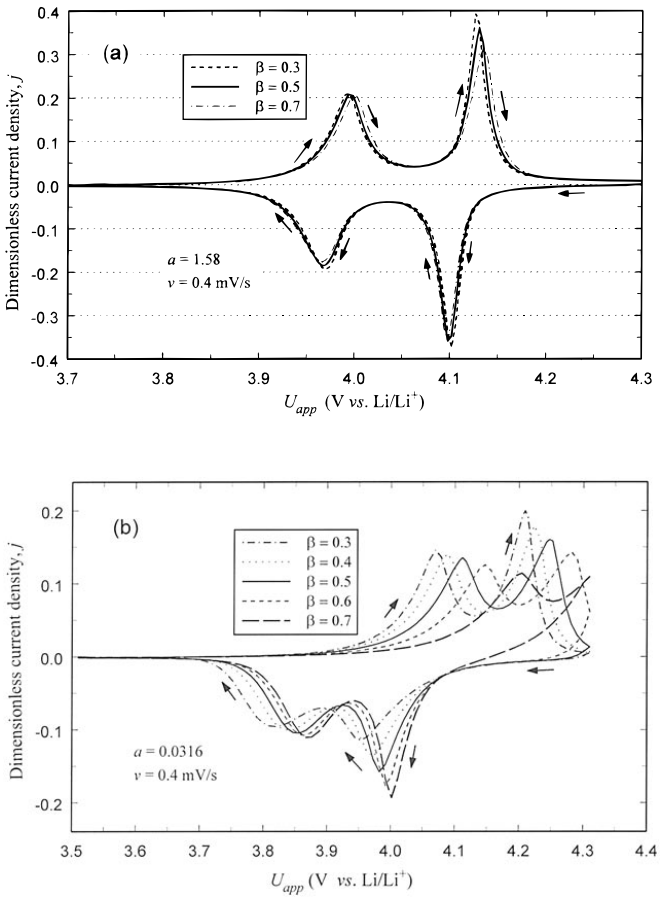

Figure 11. Cyclic voltammograms for various values of β at scan rate v = 0.4 mV/s. (a) a = 1.58 and (b) a = 0.0316.

S0013-4651(99)06-099-1 CCC: $7.00 © The Electrochemical Society, Inc.

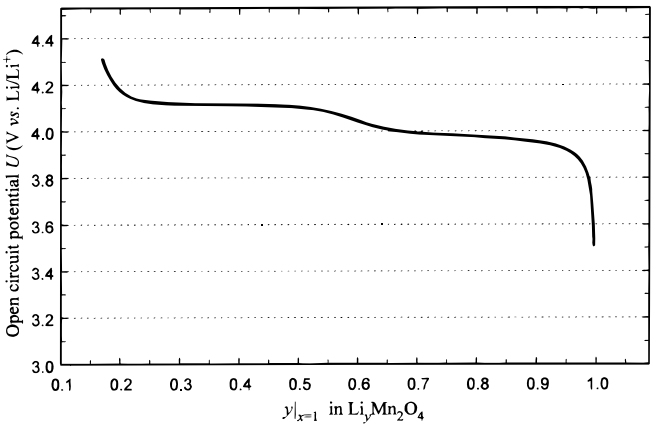

Figure A-1. The open-circuit potential as a function of dimensionless concentration $y|_{x=1}(=c_s/c_t)$ at the surface of the particle.

Summary

Cyclic voltammetric responses at different scan rates and for various values of the parameters *a* (see Eq. 24) and β (see Eq. 8) have been calculated numerically based on the mathematical model for lithium intercalation of a single spherical spinel particle. The results show that a variety of cyclic voltammograms can be predicted depending on the values of the kinetic parameters governing the electrode reaction and mass transfer in the solid. This dependence is reflected by the dimensionless group (*a*, defined in Eq. 24) that relates the transport resistance of lithium within the particle to that of interfacial electron transfer at the particle surface. The first dimensionless peak current density depends on the square root of the scan rate as given by Eq. 26 for the spinel particle studied in this present paper. Also, the peak dimensionless current density depends critically upon knowing the dependence of the open-circuit potential of the lithium-ion intercalation reaction in manganese dioxide on the dimensionless concentration (y) of Li^+ in the particle.

Acknowledgments

The authors acknowledge the financial support provided by DOE Division of Chemical Sciences, Office of Basic Energy Sciences under contract no. G.M. DE-FG02-96ER 146598, the Office of Research and Development of the United States Central Intelligence Agency under contract no. 93-F148100-000, and DOE/EPSCoR under contract no. DE-FC02-91ER75666.

The University of South Carolina assisted in meeting the publication costs of this article.

Appendix

The open-circuit potential as a function of dimensionless concentration of lithium-ions at the surface of the manganese dioxide particle is expressed as[16]

$$U = 4.19829 + 0.0565661 \tanh(-14.5546y|_{x=1} + 8.60942) - 0.0275479 [(0.998432 - y|_{x=1})^{-0.492465} - 1.90111] - 0.157123 \exp(-0.04738(y|_{x=1})^8) + 0.810239 \exp(-40y|_{x=1} + 5.355) \quad [A\text{-}1]$$

List of Symbols

a a dimensionless parameter denoting ratio of diffusional resistance of lithium in the solid host to interfacial kinetic resistance, involving the Li^+ concentration in the liquid phase, defined in Eq. 24

c concentration of lithium ions within the spinel particle, mol dm^{-3}
c_0 initial concentration of lithium ions within the spinel particle, mol dm^{-3}
c_l Li^+ concentration in the liquid electrolyte phase, mol dm^{-3}
c_s concentration of lithium ions on the surface of the spinel particle, mol dm^{-3}
c_t concentration of total sites for seating lithium ions, mol dm^{-3}
c_θ surface concentration of vacant sites ready for lithium intercalation, mol dm^{-3}
D diffusion coefficient of lithium within spinel particle, $cm^2\ s^{-1}$
F Faraday's constant, 96,487 C mol^{-1}
i deintercalation current density on particle surface, A cm^{-2}
i_0 exchange current density on particle surface, A cm^{-2}
j dimensionless current density, $j = ir_0/FDc_0$
j_p dimensionless peak current density
k interfacial charge-transfer reaction constant, $cm^{5/2}\ s^{-1}\ mol^{-1/2}$
N flux of lithium ions within particle, mol $cm^{-2}\ s^{-1}$
R universal gas constant, 8.314 J K^{-1} mol^{-1}
r radial coordinate, cm
r_0 radius of spinel particle, cm
t time, s
U equilibrium potential, V
U_0 initial applied potential, V
U_{app} applied potential, V
v potential scan rate, V s^{-1}
x dimensionless radial coordinate, $x = r/r_0$
y dimensionless concentration, $y = c/c_0$

Greek

β symmetry factor
η overpotential, V
φ potential at a point within particle, V
φ_s potential at the surface of particle, V
λ constant
θ a vacant site at the surface of spinel particle
τ dimensionless time, $\tau = tD/r_0^2$

References

1. K. West, T. Jacobsen, and S. Atlung, *J. Electrochem. Soc*., **129**, 1480 (1982).
2. Z. Mao and R. E. White, *J. Power Sources*, **43-44**, 181 (1993).
3. M. Doyle, T. F. Fuller, and J. Newman, *J. Electrochem. Soc.*, **140**, 1526 (1993).
4. T. F. Fuller, M. Doyle, and J. Newman, *J. Electrochem. Soc.*, **141**, 1 (1994).
5. B. Paxton and J. Newman, *J. Electrochem. Soc*., **143**, 1287 (1996).
6. M. W. Verbrugge and B. J. Koch, *J. Electrochem. Soc*., **143**, 24 (1996).
7. M. W. Verbrugge and B. J. Koch, *J. Electrochem. Soc*., **143**, 600 (1996).
8. H. Ura, T. Nishina, and I. Uchida, *J. Electroanal. Chem*., **396**, 169 (1995).
9. T. Nishina, H. Ura, and I. Uchida, *J. Electrochem. Soc*., **144**, 1273 (1997).
10. I. Uchida, H. Fujiyoshi, and S. Waki, *J. Power Sources*, **68**, 139 (1997).
11. R. M. Wightman, *Anal. Chem.*, **53**, 1125 (1981).
12. M. Fleischmann, S. Pons, D. R. Rolison, and P. P. Schmidt, *Ultramicroelectrodes*, Datatech Systems Inc., Morganton, NC (1987).
13. P. G. Bruce and M. Y. Saidi, *J. Electroanal. Chem*., **322**, 93 (1992).
14. K. Miura, A. Yamada, and M. Tanaka, *Electrochim. Acta*, **41**, 249 (1995).
15. H. Gerischer, in *The CRC Handbook of Solid State Electrochemistry*, P. J. Gellings and H. J. M. Bouwmeester, Editors, p. 9, CRC Press, Boca Raton, FL (1997).
16. M. Doyle, J. Newman, A. S. Gozdz, C. N. Schmutz, and J. M. Tarascon, *J. Electrochem. Soc.*, **143**, 1890 (1996).
17. S. Yamamura, H. Koshika, M. Nishizawa, T. Matsue, and I. Uchida, *J. Solid State Electrochem.*, **2**, 211 (1998).
18. G. Sewell, *Analysis of a Finite Element Method: PDE/PROTRAN*, Springer-Verlag, New York (1985).
19. D. Guyomard and J. M. Tarascon, *J. Electrochem. Soc*., **139**, 937 (1992).
20. Y. Xia and M. Yoshio, *J. Power Sources*, **56**, 61 (1995).
21. P. G. Dickens and G. F. Reynolds, *Solid State Ionics*, **5**, 53 (1981).
22. H. Kanoh, Q. Feng, Y. Miyai, and K. Ooi, *J. Electrochem. Soc*., **142**, 702 (1995).
23. H. Kanoh, Q. Feng, T. Hirotsu, and K. Ooi, *J. Electrochem. Soc.*, **143**, 2610 (1996).
24. D. Zhang, B. N. Popov, and R. E. White, *J. Power Sources*, **76**, 81 (1998).
25. P. Arora, B. N. Popov, and R. E. White, *J. Electrochem. Soc*., **145**, 807 (1998).
26. A. J. Bard and L. R. Faulkner, *Electrochemical Methods: Fundamentals and Applications*, p. 213, John Wiley & Sons, Inc., New York (1980).